

## Research Article

# Experimental Investigation of the Effect of Graphene/Water Nanofluid on the Heat Transfer of a Shell-and-Tube Heat Exchanger

Mehrdad Zolfalizadeh,<sup>1</sup> Saeed Zeinali Heris <sup>1</sup>, Hadi Pourpasha <sup>1</sup>,  
Mousa Mohammadpourfard <sup>1,2</sup> and Josua P. Meyer <sup>3</sup>

<sup>1</sup>Faculty of Chemical and Petroleum Engineering, University of Tabriz, Tabriz, Iran

<sup>2</sup>Department of Energy Systems Engineering, Izmir Institute of Technology, Izmir, Turkey

<sup>3</sup>Department of Mechanical and Mechatronic Engineering, Stellenbosch University, Stellenbosch, South Africa

Correspondence should be addressed to Saeed Zeinali Heris; [s.zeinali@tabrizu.ac.ir](mailto:s.zeinali@tabrizu.ac.ir)

Received 13 December 2022; Revised 31 January 2023; Accepted 13 February 2023; Published 2 March 2023

Academic Editor: Mahmoud Ahmed

Copyright © 2023 Mehrdad Zolfalizadeh et al. This is an open access article distributed under the Creative Commons Attribution License, which permits unrestricted use, distribution, and reproduction in any medium, provided the original work is properly cited.

The most common type of heat exchanger used in a variety of industrial applications is the shell-and-tube heat exchanger (STHE). In this work, the impact of graphene nanoplate (GNP)/water nanofluids at 0.01 wt.%, 0.03 wt.%, and 0.06 wt.% on the thermal efficiency, thermal performance factor, pressure drop, overall heat transfer, convective heat transfer coefficient (CVHTC), and heat transfer characteristics of a shell-and-tube heat exchanger was examined. For these experiments, a new STHE was designed and built. The novelty of this study is the use of GNPs/water nanofluids in this new STHE for the first time and the fully experimental investigation of the attributes of nanofluids. GNP properties were analysed and confirmed using analyses including XRD and TEM. Zeta potential, DLS, and camera images were used to examine the stability of nanofluids at various periods. The zeta potential of the nanofluids was lower than -27.8 mV, confirming the good stability of GNP/water nanofluids. The results illustrated that the experimental data for distilled water had a reasonably good agreement with Sieder-Tate correlation. The maximum enhancement in the CVHTC of nanofluid with 0.06 wt.% of GNP, was equal to 910 (W/m<sup>2</sup>K), an increase of 22.47%. Also, the efficiency of the heat exchanger for nanofluid at 0.06 wt.% improved by 8.88% compared with that of the base fluid. The heat transfer rate of the nanofluid at maximum concentration and volume flow rate was 3915 (J/kg.K), an improvement of 15.65% over the base fluid. The pressure drops increased as the flow rate and concentration of the nanofluid increased. Although increasing the pressure drop in tubes would increase the CVHTC, it would also increase the power consumption of the pump. In conclusion, nanofluid at 0.06 wt.% had good performance.

## 1. Introduction

Due to the world's limited supply of fossil fuels, optimizing energy consumption in various industrial processes has become critical. As global warming and climate change threaten human and animal survival, the usage of fossil fuels will be phased out owing to the severe environmental consequences [1]. Engineers and scientists face enormous obstacles

in fully utilising renewable energy and completely replacing it with fossil fuel consumption. Heat and energy storage have been one of the primary universal issues in building and improving techniques of devices and processes to get the most out of the energy source while minimising energy loss [2]. A heat exchanger is one of the most important devices in chemical processes for energy and heat transfer. Efforts have been made for decades to improve heat transfer, reduce heat transfer

time, reduce the size of heat exchangers, and ultimately increase energy and fuel efficiencies. These efforts include both passive and active methods, such as increasing area, using various fluids, and creating turbulence [3].

Heat exchangers (HEs) are among the most commonly used pieces of equipment in industrial processes. There are various types of HEs, including plate HEs, STHEs, and finned HEs. HEs have been used in both cooling and heating processes to transfer heat between hot and cold fluids [4]. Various parameters of HEs, such as inlet and outlet temperatures of cold and hot fluid, heat transfer characteristics, flow rate, and pressure drop of fluids, have been investigated [5].

Various fluids, such as water and ethylene glycol, and oil have been used as the operating fluids in HEs. But these fluids have low thermophysical values compared with those of nanofluids. Nanofluid with high thermophysical attributes can be used instead of base fluids [4]. Dispersed nanoparticles in a pure fluid with suitable thermophysical specifications such as thermal conductivity and heat capacity have been used as a nanofluid to improve heat transfer. Nowadays, in several scientific fields, nanoparticles with nanosized particles smaller than 100 nm have been extensively examined [6]. Also, metal nanoparticles such as Ag [7], Cu [8], and Al [9], metal oxide such as  $\text{Fe}_3\text{O}_4$  [10, 11],  $\text{Al}_2\text{O}_3$  [12], and  $\text{TiO}_2$  [13], carbon-based nanoparticles such as graphene [14], and multiwalled carbon nanotubes (MWCNTs) [15] are among the most common nanoparticles. For enhancing heat transfer, graphene and carbon nanotubes have greater thermophysical characteristics than other nanomaterials. The graphene-based nanoparticles possess higher thermal conductivity and have better properties such as low erosion, corrosion, higher stability, and hence, it is preferred in various the heat exchangers [16]. Top-down and bottom-up approaches can be used to synthesise nanoparticles [17]. The top-down method is viewed as a physical process that includes the breakdown of most of the substance into nanoparticles using techniques such as acid etching [18], ball milling [19], and laser ablation [20]. In contrast, the bottom-up approach uses chemical precursors to create nanoparticles. This group consists of solvothermal techniques [21], microemulsion [22], sol-gel procedures [23], and coprecipitation [24]. By distributing the nanoparticles into the base fluid in a two-step or one-step process, nanofluids can be synthesised [25].

The studies analysed below investigated the impact of nanoadditives on the heat transfer of water in HEs. Ghozatloo et al. [26] examined the impact of a graphene/water nanofluid on convective heat transfer in STHE. The maximum thermal conductivity of a nanofluid at a concentration of 0.075 wt.% was improved by 29.2% at a temperature of 25°C. The CVHTC of the nanofluid improved by 25.6% for a concentration of 0.1 wt.% at a temperature of 38°C compared with that of the base fluid. Selvam et al. [27] investigated the optimisation of the overall heat transfer coefficient (OHTC) with graphene-based suspensions in automobile radiators. The results illustrated that the thermal conductivity coefficient improved from 0.465 at 30°C to 0.615 at 50°C. The viscosity increased from 1.622 to 1.845

at 30°C and from 1.065 to 1.488 at 50°C. Also, the maximum improvements of the OHTC for a nanofluid with 0.5 vol.% of nanoparticles at 35°C and 45°C with a flow rate of 62.6 g/s were 104% and 81%, respectively. Wang et al. [28] experimentally studied graphene/water nanofluid cooling in a miniature plate heat exchanger. Their findings indicated that the thermal conductivity coefficient was improved by 17% and 21.1%, and the viscosity was increased by 200%. Also, the CVHTC improved up to 4% by increasing the concentration from 0.01% to 0.1%. Esfahani and Languri [29] analysed the performance of graphene oxide nanofluid in an STHE. The thermal conductivity coefficient of graphene oxide/water nanofluid in concentrations of 0.01 wt.% and 0.1 wt.% at a temperature of 25°C increased by 9% and 20%, respectively. Kumar and Sonawane [30] investigated the improvement of heat transfer in an STHE for laminar and turbulent flow by  $\text{Fe}_2\text{O}_3$ /water and  $\text{Fe}_2\text{O}_3$ /ethylene glycol nanofluids. The use of both nanofluids improved the CVHTC and the OHTC. In addition, the pressure drop increased in turbulent flow, unlike laminar flow. Barzegarian et al. [31] investigated the use of  $\text{Al}_2\text{O}_3$ /water nanofluid to improve the thermal performance of horizontal STHE in forced circulation. Their findings illustrated that the Nusselt number (Nu) and the OHTC increased with the increment of the Reynolds number (Re). Also, the thermal performance coefficient at a concentration of 0.3% improved by 21.5%. Shahrul et al. [32] investigated the heat performance of water-based nanofluids of  $\text{Al}_2\text{O}_3$ ,  $\text{SiO}_2$ , and ZnO nanoparticles in a STHE. The highest CVHTC, OHTC, and actual heat transfer have been observed for ZnO–water, and the lowest effectiveness, highest CVHTC, OHTC, and actual heat transfer have been found for  $\text{SiO}_2$ –water. Approximately, 50%, 15%, and 9% enhancement in the highest convective heat transfer coefficient has been found for ZnO–water,  $\text{Al}_2\text{O}_3$ –water, and  $\text{SiO}_2$ –water nanofluids, respectively. Hassaan [33] investigated the heat transfer performance of a STHE using MWCNT/water nanofluid. Their results indicated that the Nu increased by up to 55.6% when the volume concentration percentage was 2%, which is the highest increase, 19.4%–38.7% increase in effectiveness when using MWCNTs nanofluids instead of distilled water with a volume concentration up to 2%. Taghizadeh-Tabari et al. [34] investigated the thermal behaviour of  $\text{TiO}_2$ /water nanofluid in plate heat exchangers.  $\text{TiO}_2$  nanoparticles were added to the distilled water to prepare stable nanofluid with concentrations of 0.25 wt.%, 0.35 wt.%, and 0.8 wt.% as the working fluid. Their results indicated that using nanofluids at all concentrations increased the heat transfer rate (an advantage) and pressure drop (a disadvantage) compared with distilled water. Heris et al. [35] studied heat transfer of a car radiator with CuO/ethylene glycol-water as a coolant. The experiment was performed for different volumetric concentrations (0.05–0.8 vol.%) of nanofluids at different flow rates (4–8 lit/min) and inlet temperatures (35, 44, and 54°C). The results illustrated that nanofluids clearly enhanced heat transfer compared with the base fluid. An HTC enhancement of about 55% compared with the base fluid was obtained.

The novelty of the present study is the use of GNPs/water nanofluids in type of STHE and the investigation of their relevant properties using experimental methods and equations. Various related studies have recently investigated the use of other nanoparticles and water nanofluids in STHEs, but the impact of GNPs on the performance of STHEs has not been studied yet. The goal of this research was to improve heat transfer by designing and manufacturing new STHEs and incorporating GNP as an additive.

In this study, the impact of mass fractions of nanoparticles (0.01, 0.03, and 0.06 wt.%) and various inlet velocities on Nu, heat transfer rate, CVHTC, OHTC, and pressure drop were investigated. More importantly, the thermal efficiency of STHE, and the thermal performance factor were investigated. Finally, the optimum and best results were provided.

## 2. Material and Methods

**2.1. Nanofluid Synthesis.** For the synthesis of the GNP/water nanofluid, GNPs (purity of 99.9%) were purchased from VCN Materials Co. Table 1 shows the characteristics of GNPs. Distilled water was used as a base fluid (density: 998 kg/m<sup>3</sup>, specific heat: 4200 (J/kg.K), thermal conductivity: 0.607 (W/m.K), and viscosity: 0.89 (cP) at 25°C). Gum Arabic (GA) surfactant was used as a surfactant at a ratio of 2:1. The surfactant was added to the distilled water and mechanically mixed with a stirrer mixer at 1 200 rpm for 30 minutes. Then, GNPs were added to the solution and blended for 60 minutes. To prepare stable nanofluids, an ultrasound probe (550 watts) was used for 15 minutes to improve the stability of nanofluids. Finally, GNP-water nanofluids were prepared in concentrations of 0.01, 0.03, and 0.06 wt.%.

**2.2. Experimental Set-Up.** Figure 1 depicts the experimental set-up, which consisted of an STHE, four PT100 thermocouples with 0.1% precision, four temperature controllers to indicate temperatures with 0.1% accuracy, a 3000 W coil heater element, a nanofluid reservoir tank, two drain containers, and a circulator pump. Nanofluid as a hot fluid in a closed loop and tap water as a cold fluid at the countercurrent flow condition flowed along the tube side and shell side of the heat exchanger, respectively. The heat of the hot fluid was supplied by a coil heater element in the reservoir tank and was pumped to the heat exchanger by the circulator pump. Then, it returned to the reservoir tank. In addition, a bypass path was incorporated to control the flow rate of hot fluid. The detailed specifications of the designed STHE are provided in Table 2. For testing, nanofluids were prepared in concentrations of 0.01, 0.03, and 0.06 wt.%. Nanofluid was used as a hot fluid and water as a cold fluid. The cold fluid flow rate was considered constant. After the experimental system reached steady state, flow rates of both inlet and outlet hot fluid, as well as temperatures of inlet and outlet hot and cold fluid, were recorded for each test condition. According to the obtained experimental data, the HTC, Nu, and Pe were calculated.

**2.3. Characterisation Methods.** In this study, the composition of nanoparticles and the functional groups present on

the surface of nanoparticles were analysed using X-ray diffraction (XRD). The morphology of nanoparticles, such as their form and size, was studied using transmission electron microscopy (TEM). The particle size distribution of nanofluids was investigated using dynamic light scattering (DLS). The stability of nanofluids was investigated by zeta potential.

**2.4. Equations.** The following equations were used to calculate the thermophysical and thermal characteristics of nanofluids.

The thermal conductivity of nanofluid was estimated using Yu and Choi's [36] model. In addition to the thermal conductivity of the base fluid and nanoparticles and the nanoparticle volume fraction, this equation also considered the effect of the interface between fluid and solid nanoparticles in obtaining the thermal conductivity coefficient:

$$K_{nf} = \left[ \frac{K_{np} + 2K_{bf} + 2(K_{np} - K_{bf})(1 + \beta)^3 \varphi}{K_{np} + 2K_{bf} - (K_{np} - K_{bf})(1 + \beta)^3 \varphi} \right] K_{bf}, \quad (1)$$

where  $k_{bf}$  is the thermal conductivity of the base fluid,  $k_{np}$  is the thermal conductivity of nanoparticles,  $\varphi$  is the volume concentration of nanoparticles, and  $\beta$  is the ratio of the nanolayer thickness to the original particle radius. The Pak and Cho equation [37] was used to evaluate the density of nanofluid, as follows:

$$\rho_{nf} = (1 - \varphi)\rho_{bf} + \varphi \cdot \rho_{np}, \quad (2)$$

where  $\rho_{bf}$  is the density of base fluid and  $\rho_{np}$  is the density of nanoparticles. The Brinkman equation [38] was used to calculate fluid viscosity for average particle concentration:

$$\mu_{nf} = \frac{\mu_{bf}}{(1 - \varphi)^{2.5}}, \quad (3)$$

where  $\mu_{bf}$  is the viscosity of the base fluid. The specific heat capacity ( $C_p$ ) of nanofluid was calculated by Xuan and Roetzel [39], as follows:

$$(\rho C_p)_{nf} = \varphi(\rho C_p)_{np} + (1 - \varphi)(\rho C_p)_{bf}, \quad (4)$$

where  $C_{p_{np}}$  and  $C_{p_{bf}}$  are the specific heat capacity of nanoparticles and base fluid, respectively. The mean HTC ( $\bar{h}$ ) was calculated by the following equations [40]:

$$\bar{T}_h = \frac{T_{h_{in}} + T_{h_{out}}}{2}, \quad (5)$$

$$\bar{T}_c = \frac{T_{c_{in}} + T_{c_{out}}}{2}, \quad (6)$$

$$Q = \bar{h}A\bar{\Delta T} = \dot{m}_{nf}C_{p_{nf}}\Delta T_{nf}, \quad (7)$$

where  $\bar{T}_h$  and  $\bar{T}_c$  are the mean hot and cold fluid temperatures, respectively.  $T_{h_{in}}$ ,  $T_{h_{out}}$ ,  $T_{c_{in}}$ , and  $T_{c_{out}}$  are inlet hot fluid

TABLE 1: Graphene nanoplatelet properties.

Nanoparticle	Density (g/cm <sup>3</sup> )	Morphology	Diameter (μm)	Thickness (nm)	Purity/%
Graphene	1.9-2.2	Platelet	1-20	<40	99.9

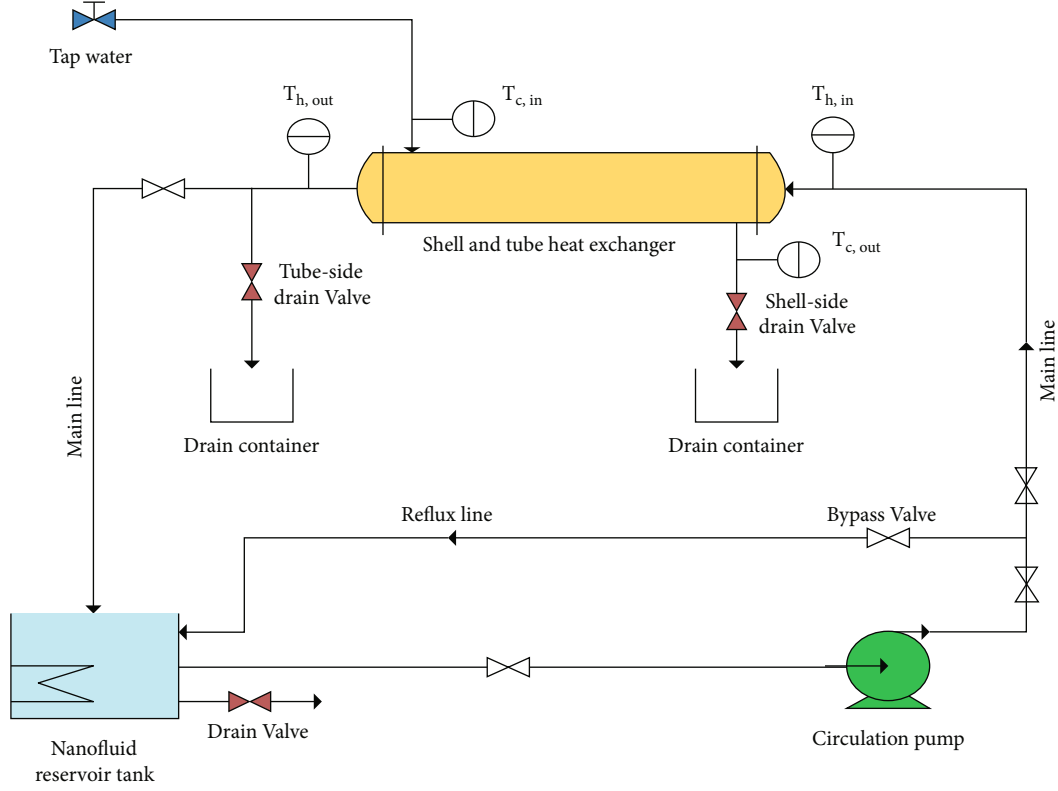


FIGURE 1: Schematic of experimental set-up.

TABLE 2: Specifications and operating conditions of experimental set-up.

Description	Specifications
Type of heat exchanger	Single pass
Tube material	Copper
Tube outside diameter, $d_o$	8 mm
Tube inside diameter, $d_i$	7 mm
Number of tubes, $N$	16
Tube length, $l$	430 mm
Tube arrangement	Triangular
Shell material	St37 steel
Shell outside diameter, $D_o$	100 mm
Shell inside diameter, $D_i$	92 mm
Baffle type	Single-segmental
Baffle cut	25%
Number of baffles	5
Nanofluid mass flow rate (kg/s)	0.020-0.065
Water mass flow rate (kg/s)	0.083
Nanofluid temperature in tank	Approx. 80°C
Water temperature	Approx. 20°C

temperature, outlet hot fluid temperature, inlet cold fluid temperature, and outlet cold fluid temperature, respectively.  $Q$  is the heat transfer rate, and  $A$  is the heat transfer area;  $\overline{\Delta T}$  is the mean temperature difference between hot and cold fluids;  $\dot{m}_{nf}$  is the mass flow rate of nanofluid, and  $\Delta T_{nf}$  is the temperature difference between inlet and outlet nanofluid. Mean Nu of nanofluid is defined as [41]:

$$\overline{Nu}_{nf} = \frac{\bar{h}D}{k_{nf}}, \quad (8)$$

where  $D$  is the hydraulic diameter of the tube and  $K_{nf}$  is the thermal conductivity of nanofluid. Re and Prandtl number (Pr) of nanofluid were calculated by the following equations [41, 42]:

$$Re_{nf} = \frac{\rho_{nf} u D}{\mu_{nf}}, \quad (9)$$

$$Pr_{nf} = \frac{C_{p,nf} \mu_{nf}}{k_{nf}}. \quad (10)$$

Pe of nanofluid could be defined as [43]:

$$Pe_{nf} = Re_{nf} Pr_{nf}. \quad (11)$$

The OHTC of the shell-and-tube heat exchanger was calculated based on the following correlation [44]:

$$U = \frac{Q}{A.LMTD}, \quad (12)$$

where  $Q$  was calculated by Equation (7). Also,  $A = N\pi DL$  and  $LMTD$  are the heat transfer area and the logarithmic mean temperature difference, respectively.  $N$  is the number of tubes;  $D$  is hydraulic diameter of the tube; and  $L$  is the length of the tubes.

The Darcy-Weisbach equation for laminar flow was used for the determination of pressure drop in heat exchanger tubes, as follows [42]:

$$\frac{\Delta P}{L} = \frac{128 \mu \dot{V}}{\pi D^2}, \quad (13)$$

where  $\dot{V}$  is the volumetric flow rate. The efficiency of the STHE is defined as the ratio of the actual heat transfer to the ideal value of heat transfer and is shown by the following equation [45]:

$$\varepsilon = \frac{(T_{h_{in}} - T_{h_{out}})}{(T_{h_{in}} - T_{c_{in}})}. \quad (14)$$

The thermal performance factor ( $\eta$ ) is defined as the ratio of the enhanced heat transfer to the increased friction. The thermal performance factor ( $\eta$ ) can be written as [46]:

$$\eta = \frac{(Nu_{nf}/Nu_{bf})}{(f_{nf}/f_{bf})^{1/3}}, \quad (15)$$

where  $Nu_{nf}$  is the Nusselt number of nanofluid,  $Nu_{bf}$  is the Nusselt number of base fluids,  $f_{nf}$  is the nanofluid friction, and  $f_{bf}$  is the base fluid friction.

**2.5. Uncertainty Analysis.** Each measured parameter has a measurement error. To calculate the uncertainty ( $U_{R_i}$ ) of any parameter such as  $R$ , the uncertainty interval for independent experimentally measured variables ( $x_i$ ) could be estimated by the following equation [41]:

$$U_{R_i} = \frac{X_i}{R} \frac{\partial R}{\partial X_i} U_{X_i}, \quad (16)$$

where  $U_{R_i}$  is the maximum error in calculating a parameter,  $X_i$  is the measurable parameter,  $U_{X_i}$  is the measurement error, and  $R$  is the quantity calculated from measurable parameters.

For example, the uncertainty of nanofluid volume measurement in the reservoir is  $U_{vol} = \pm(1/300) = \pm 3.3 \times 10^{-3}$ , the uncertainty of time measurement for reservoir filling is  $U_t = \pm((0/05)/(4/6)) = \pm 1.1 \times 10^{-2}$ , respectively.

TABLE 3: The uncertainties of different parameters.

Parameter	Uncertainty
$D$	0.00625
$L$	0.023
$\mu_{nf}$	0.0025
$\rho_{nf}$	0.0025
$K_{nf}$	0.0035
$C_{p_{nf}}$	0.0025
$u_{nf}$	0.0126
$(T_{h_{in}} - T_{h_{out}})$	0.00237
$(\bar{T}_h - \bar{T}_c)$	0.00453

Due to the combined effect of uncertainty intervals in all values of  $x_i$  ( $i = 1, 2, \dots, n$ ) the uncertainty in  $R$  can be calculated by [45]:

$$\text{Max. } U_R = \pm \left[ \left( \frac{X_1}{R} \frac{\partial R}{\partial X_1} U_{X_1} \right)^2 + \left( \frac{X_2}{R} \frac{\partial R}{\partial X_2} U_{X_2} \right)^2 + \dots + \left( \frac{X_n}{R} \frac{\partial R}{\partial X_n} U_{X_n} \right)^2 \right]^{1/2}. \quad (17)$$

In Equation (17),  $U_R$  is the maximum error of final parameters.

The uncertainty of the measured parameters was determined by dividing the measurement accuracy by the minimum measured value over the experiments. Consequently, maximum uncertainty for input heat transfer coefficient, heat transfer rate, Nusselt number, flow rate, and Reynolds number can be calculated as follows:

$$\text{Max. } U_{\bar{h}(\text{exp})_{nf}} = \pm \left[ \begin{aligned} &U_{\rho_{nf}}^2 + U_{U_A}^2 + U_{C_{p_{nf}}}^2 + \left( U_{(T_{h_{in}} - T_{h_{out}})} \right)^2 + \\ &(-U_D)^2 + (-U_L)^2 + \left( -U_{(\bar{T}_h - \bar{T}_c)} \right)^2 \end{aligned} \right]^{1/2} = \pm 0.027 \approx 2.7\%, \quad (18)$$

$$\text{Max. } U_{Q_{\bar{h}(\text{exp})}} = \pm \left[ U_{\rho_{nf}}^2 + U_{U_A}^2 + U_{C_{p_{nf}}}^2 + \left( U_{(T_{h_{in}} - T_{h_{out}})} \right)^2 \right]^{1/2} = \pm 0.012 \approx 1.2\%, \quad (19)$$

$$\text{Max. } U_{\overline{Nu}(\text{exp})_{nf}} = \pm \left[ U_{\bar{h}(\text{exp})_{nf}}^2 + U_D^2 + (-U_{K_{nf}})^2 \right]^{1/2} = \pm 0.028 \approx 2.8\%, \quad (20)$$

$$\text{Max. } U_{\bar{U}_A} = \pm \left[ U_{vol}^2 + (-U_t)^2 \right]^{1/2} = \pm 0.011 \approx 1.1\%, \quad (21)$$

$$\text{Max. } U_{Re} = \pm \left[ U_{\rho_{nf}}^2 + U_{u_{nf}}^2 + U_D^2 + \left( -U_{\mu_{nf}} \right)^2 \right]^{1/2} = \pm 0.015 \approx 1.5\%. \quad (22)$$

Therefore, the uncertainties in heat transfer coefficient, heat transfer rate, and Nusselt number are  $\pm 2.7\%$ ,  $\pm 1.2\%$ , and  $\pm 2.8\%$ , respectively. The uncertainties of the necessary parameters are summarized in Table 3.

**2.6. Data Validation.** In order to compare and check the accuracy of the experimental set-up for the correct determination of the CVHTC, experiments were performed with distilled water as the base fluid before starting the experiment with nanofluid. For this purpose, the following experimental equations were used for the fluid inside the tube in laminar flow to compare experimental and calculated Nu. The Sieder-Tate equation (Equation (23)) was used to validate [46]:

$$\text{Nu} = 1.86 \left( \text{Re}_{\text{nf}} \text{Pr}_{\text{nf}} \frac{D}{L} \right)^{1/3} \left( \frac{\mu_b}{\mu_w} \right)^{0.14} \left( \text{Re}_{\text{nf}} \text{Pr}_{\text{nf}} \frac{D}{L} \right) > 10, \quad (23)$$

where  $D$  is the internal diameter of the tube,  $\mu_b$  is the fluid viscosity at the bulk mean temperature, and  $\mu_w$  is the fluid viscosity at the tube-wall surface temperature. The Shah equations (Equation (24) and Equation (25)) [47] and Hausen equation (Equation (26)) [48] were used to validate:

$$\text{Nu} = 1.953 \left( \text{Re}_{\text{nf}} \text{Pr}_{\text{nf}} \frac{D}{L} \right)^{1/3}, \text{ for } \left( \text{Re}_{\text{nf}} \text{Pr}_{\text{nf}} \frac{D}{L} \right) \geq 33.3, \quad (24)$$

$$\text{Nu} = 4.364 + 0.0722 \left( \text{Re}_{\text{nf}} \text{Pr}_{\text{nf}} \frac{D}{L} \right), \text{ for } \left( \text{Re}_{\text{nf}} \text{Pr}_{\text{nf}} \frac{D}{L} \right) < 33.3, \quad (25)$$

$$\text{Nu} = 3.66 + \frac{0.0668(D/L) \text{Re}_{\text{nf}} \text{Pr}_{\text{nf}}}{1 + 0.04[(D/L) \text{Re}_{\text{nf}} \text{Pr}_{\text{nf}}]^{2/3}}. \quad (26)$$

Figure 2(a) indicates that the calculated data for distilled water was in good agreement with the Sieder-Tate equation. Considering the results obtained in Figure 2(b), the experimental data for distilled water had a reasonably good agreement with Sieder-Tate correlation. The standard deviation of the calculated data for Sieder-Tate correlation based on the experimental data is indicated in Figure 2(b). As shown in Figure 2(b), the maximum standard deviation between the calculated and experimental Nu for distilled water was 14%, which emphasises the accuracy and reliability of the experiments.

### 3. Experimental Results

**3.1. Nanoparticle Characteristics and Stability of Nanofluid.** TEM images of GNPs are shown in Figures 3(a) and 3(b). The planar and layered structures of the GNPs sample, along with the wrinkles on the surface layer, were clearly defined. An XRD analysis was used to identify the structure and crystallography of GNPs. The XRD analysis pattern of GNPs is shown in Figure 3(c). As shown in Figure 3(c), there were two peaks at  $26.77^\circ$  ( $d$ -space =  $3.3302 \text{ \AA}$ ) and  $44.23^\circ$  ( $d$ -space =  $2.048 \text{ \AA}$ ). The peaks appearing at  $26.77^\circ$  and  $44.23^\circ$  corresponded to the diffraction from (002) and (100) planes, respectively [49, 50], indicating the crystalline and layered structure of GNPs in relation to the diffraction from the graphite phase. The sharp and long peak (002) shows that

the formed GNPs was not a single layer and had a completely crystalline structure of carbon base, and the broad peak (100) confirms that the GNP sheets were layered.

Figure 4(a) illustrates the DLS analysis of GNP/water nanofluids at various concentrations (0.01, 0.03, and 0.06 wt.%). The particle (as cluster) size distribution of GNP obtained at 0.01 wt.% was 6.79% of 72.3 nm, 16.03% of 85.9 nm, 26.16% of 102.2 nm, 20.7% of 121.5 nm, 14.78% of 144.5 nm, 10.23% of 171.9 nm, and 5.31% of 204.4 nm. The particle (as cluster) size distribution of GNP obtained at 0.03 wt.% was 4.32% of 85.9 nm, 12.53% of 102.2 nm, 25.66% of 121.5 nm, 26.2% of 144.5 nm, 16.28% of 171.9 nm, and 4.28% of 243 nm. The particle (as cluster) size distribution of GNP obtained at 0.06 wt.% was 10.01% of 121.5 nm, 20.24% of 144.5 nm, 29.11% of 171.9 nm, 24.43% of 204.4 nm, 12.27% of 243 nm, and 3.94% of 289 nm. According to the findings, adding GNP to water increased the size of the cluster. Zeta potential analyses of GNP/water nanofluids at various concentrations (0.01, 0.03, and 0.06 wt.%) are shown in Figure 4(b). Analyses indicated that the stability of GNP/water nanofluids decreased as the nanoparticle concentration increased. Because there was no tendency for mutual repulsion between the particles, this could be due to the aggregation of nanoparticles with a high surface charge. The accumulation of particles, on the other hand, reduced both the dispersion of nanoparticles and the stability of the nanofluid. Furthermore, with an increase in concentration of more than 0.03 wt.%, a downward trend in the stability of the nanofluid was observed, indicating that the optimal value of that concentration had been determined. However, at these nanoparticle mass fractions, the zeta potential of the nanofluids was lower than  $-27.8 \text{ mV}$ , confirming the good stability of GNP/water nanofluids. Figure 5 presents camera pictures of nanofluids at various mass fractions (0.01, 0.03, and 0.06) after 1 h, 7 days, 14 days, and 30 days of synthesis. The nanofluids containing GNP at 0.01 wt.% and 0.03 wt.% were stable for 30 days. After 7 days, a nanofluid containing 0.06 wt.% GNP precipitated, as shown in Figure 5(f). Figures 5(i) and 5(l) demonstrate the precipitation of nanofluids containing 0.06 wt.% over a 14-day and 30-day period, respectively. Visual observations showed that nanofluids with lower concentrations of 0.01 wt.% and 0.03 wt.% had good stability for up to 30 days with only minor precipitation (Figures 5(j) and 5(k)).

**3.2. Convective Heat Transfer of Nanofluids.** After preparation of the nanofluids at concentrations of 0.01 wt.%, 0.03 wt.%, and 0.06 wt.%, the heat transfer measurement tests for obtaining Nu, heat transfer rate, CVHTC, OHTC, pressure drop, thermal efficiency, and thermal performance factor were conducted. Figure 6(a) shows the CVHTC of GNP/water nanofluids with varying GNP mass fractions and Re. The CVHTC increased as Re increased, as shown in Figure 6(a). With an increase in nanofluid concentration, the CVHTC also increased. This increase was due to the increase in thermal conductivity and decrease in boundary layer thickness as a result of the increase in flow turbulence. The maximum value of the CVHTC at a nanofluid concentration of 0.06 wt.% was  $910 \text{ (W/m}^2\text{.K)}$ . In addition, the

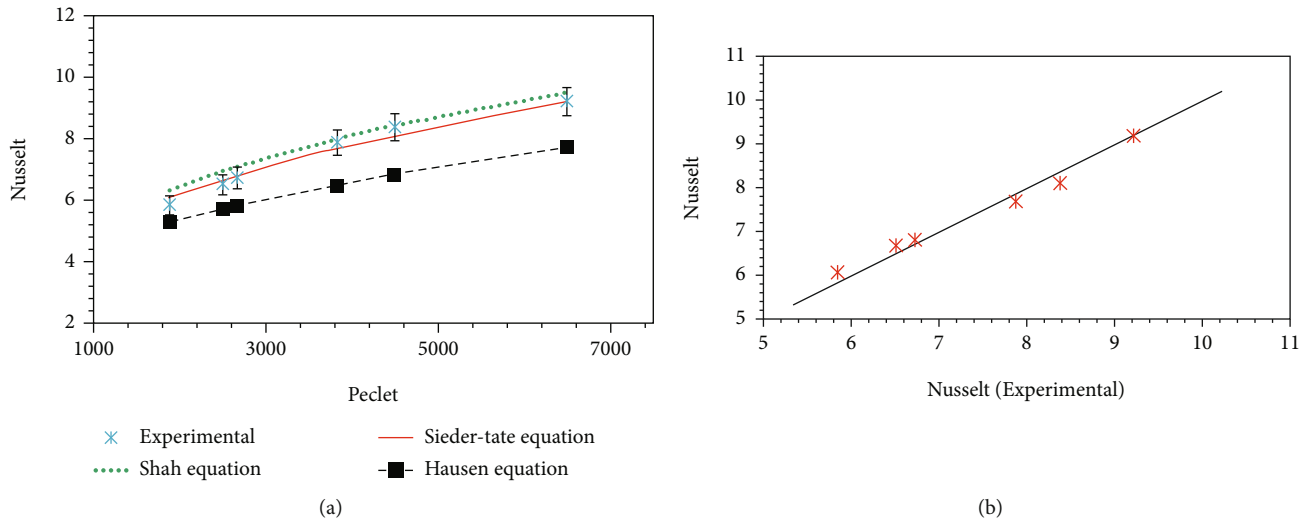


FIGURE 2: (a) Variations of calculated and experimental Nu for distilled water versus Pe in experimental set-up and (b) comparison between calculated and experimental Nu for distilled water in experimental set-up by Sieder-Tate equation.

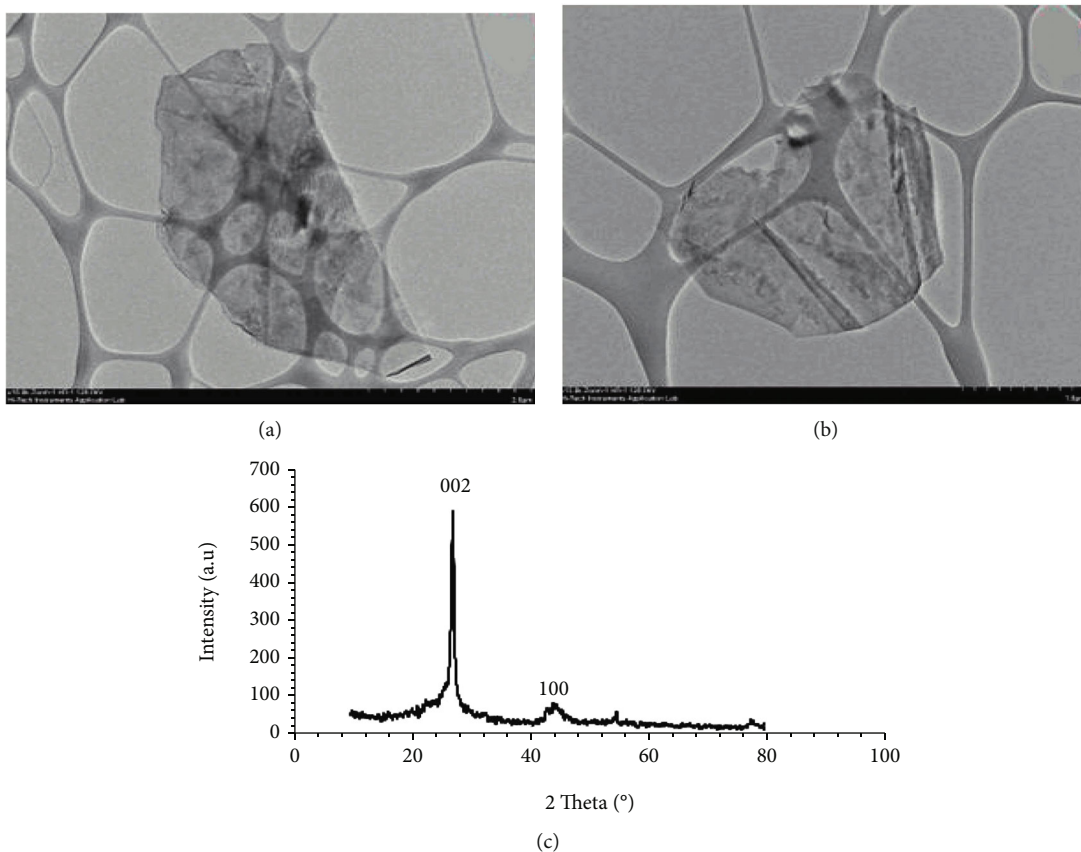


FIGURE 3: (a, b) TEM images of GNPs and (c) XRD analysis pattern of GNPs.

CVHTC improved by 22.47% at the highest concentration value of 0.06 wt.% compared with the base fluid. Ghozatloo et al. [26] indicated the CVHTC of the nanofluid improved by 25.6% for a concentration of GNPs at 0.1 wt.% compared with that of the base fluid. Wang et al. [28] reported that the

CVHTC improved up to 4% by increasing the concentration of GNPs from 0.01% to 0.1%. Fares et al. [51] reported that a maximum increase in the heat transfer coefficient of 29% was achieved using 0.2% GNPs/water nanofluids. Furthermore, the mean thermal efficiency of the heat exchanger

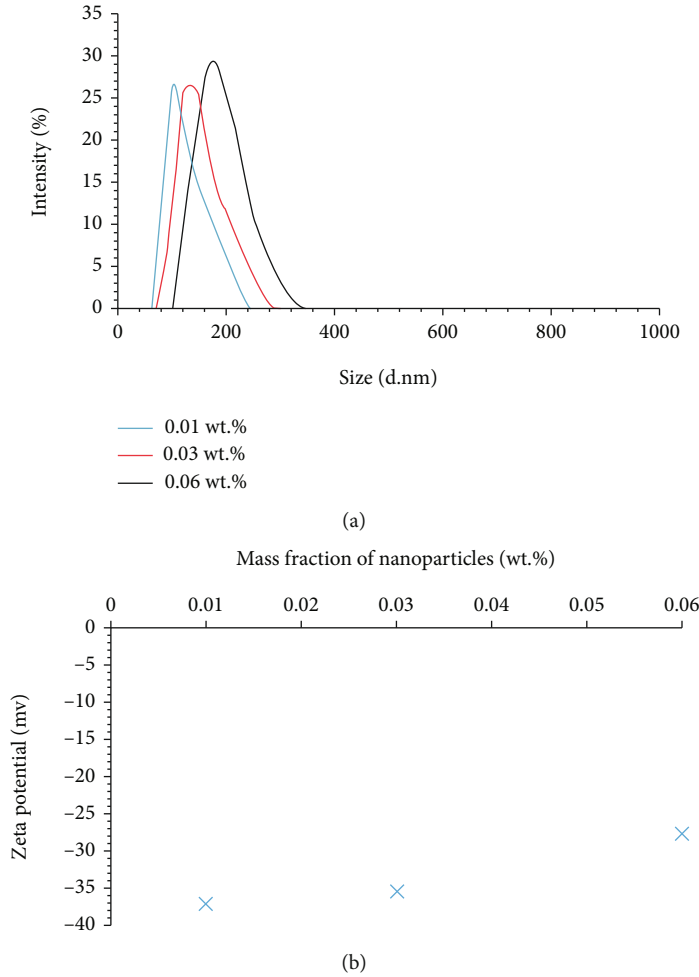


FIGURE 4: (a) DLS analysis of GNP/water nanofluids at various concentrations and (b) zeta potential analyses of GNP/water nanofluids at various concentrations.

was enhanced by 13.7% by using GNPs/water nanofluid. Compared to the researchers' studies, in this study, better results were achieved by designing and building a new heat exchanger using nanoparticles at lower concentrations of GNP. The effect of various Re on Nu for nanofluids with various concentrations is shown in Figure 6(b). As a result, the Nu increased with increasing Re and improved with increasing nanofluid concentration. The highest value of Nu at a concentration of 0.06 wt.% was 11. In addition, the Nu for nanofluid at a concentration of 0.06 wt.% improved by 12.36% compared with that of the base fluid. Figure 6(c) depicts the relationship between OHTC in STHE using GNP/water nanofluid and flow rate for various GNP loadings. The OHTC improved with increasing volumetric flow rate and nanofluid concentration, as shown in Figure 6(c). This trend was due to the increment of the CVHTC leading to an increase in heat transfer rate and OHTC. This increase can be seen clearly in Figure 6(d), which shows that with the increasing volumetric flow rate and concentration of nanofluid, the heat transfer rate increased. The heat transfer rate of the nanofluid at maximum concentration and volume flow rate was 3915 (J/kg.K), an improvement of 15.65% over the base fluid.

**3.3. Pressure Drops, Thermal Efficiency, and Thermal Performance Factor.** Figure 7(a) indicates the impact of different flow rates on the pressure drop along tube length and for nanofluids with various concentrations. The pressure drops increased as the flow rate and concentration of the nanofluid increased. Although increasing the pressure drop in tubes would increase the CVHTC, it would also increase the power consumption of the pump. Also, the increase in pressure drops caused corrosion in the inner part of the tube. Figure 7(b) is a comparison between the thermal efficiency of STHE and the Re. The system's efficiency decreased as Re increased. The residence time of nanofluid in tubes decreased as Re increased. Furthermore, decreasing the resident time of nanofluid decreased the temperature difference between the inlet and outlet of nanofluid. In addition, with an increase in nanofluid concentration, the thermal efficiency of the system increased, and the highest value at a concentration of 0.06 wt.% was 0.49, which was improved by 8.88% compared with that of the base fluid. Figure 7(c) depicts the effects of Re and GNP concentrations on the thermal performance factor. The thermal performance coefficient behaved differently as the Re increased, as shown in Figure 7(c). At low Re and a concentration of

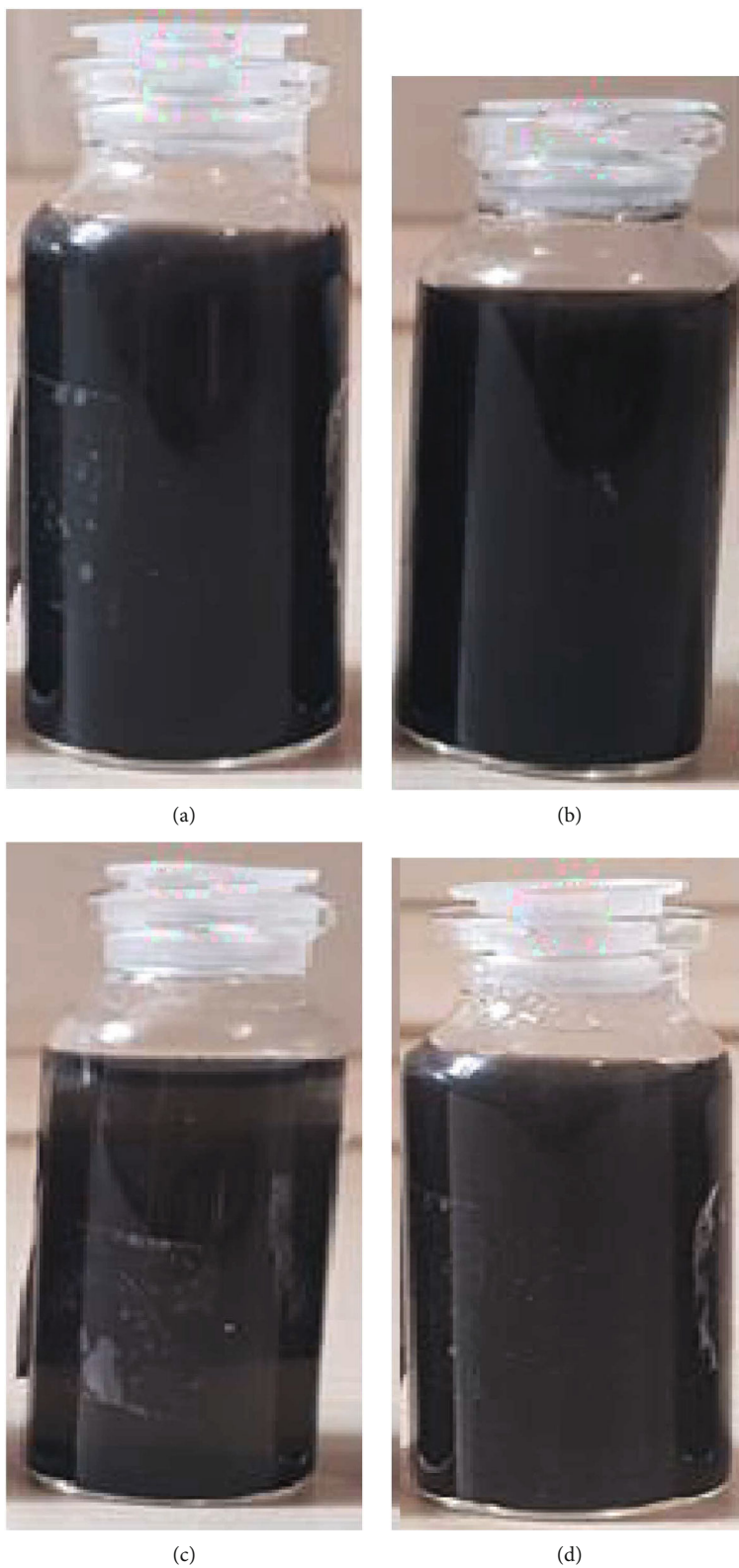


FIGURE 5: Continued.



(e)



(f)



(g)



(h)

FIGURE 5: Continued.

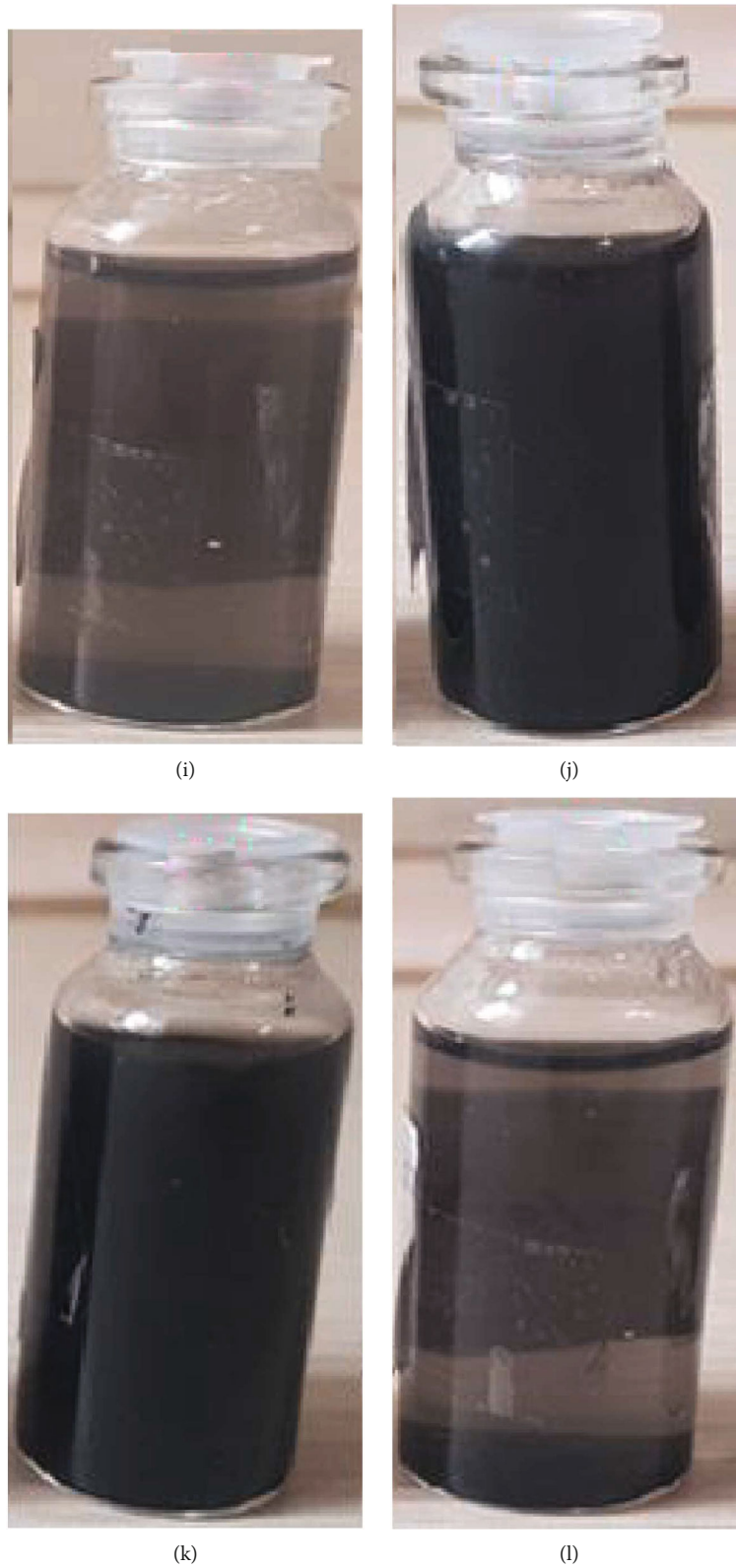


FIGURE 5: Camera pictures of nanofluids at various mass fractions (0.01, 0.03, and 0.06) after 1 h, 7 days, 14 days, and 30 days of synthesis.

0.01 wt.%, the thermal performance factor increased with increasing Re due to the low density and viscosity of the nanofluid. At concentrations of 0.03 wt.% and 0.06 wt.%, with increasing concentrations of nanoparticles, the friction

factor and pressure drop increased, which led to a decrease in the performance factor. However, for Re of 480 to 630, the performance factor decreased for all three concentrations of nanoparticles due to an increase in pressure drop.

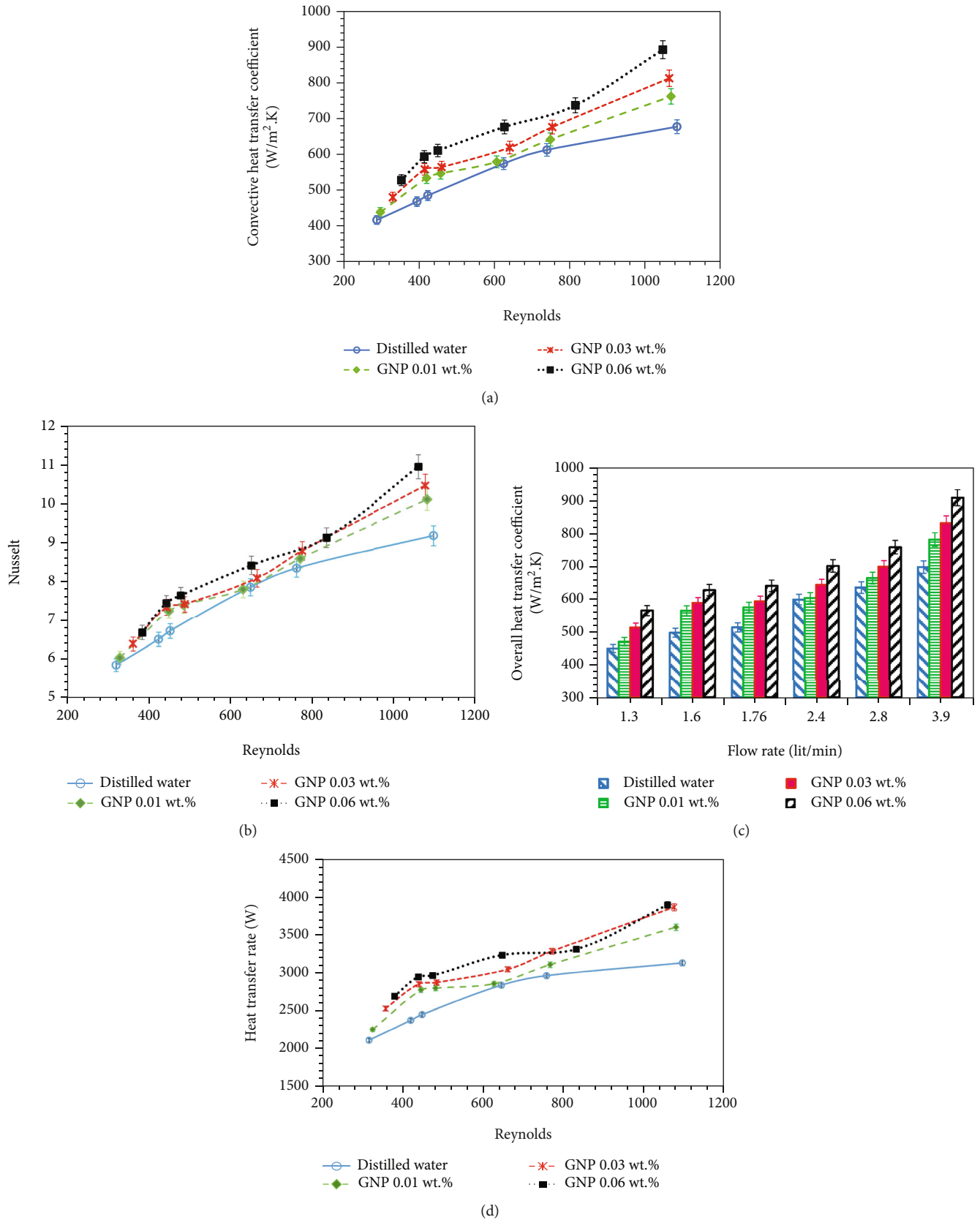


FIGURE 6: (a) CVHTC of GNP/water nanofluid versus  $Re$  for different concentrations, (b)  $Nu$  for GNP/water nanofluid versus  $Re$  for various concentrations, (c) OHTC for GNP/water nanofluid versus flow rate at different concentrations, and (d) heat transfer rate for GNP/water nanofluid versus  $Re$  for various concentrations.

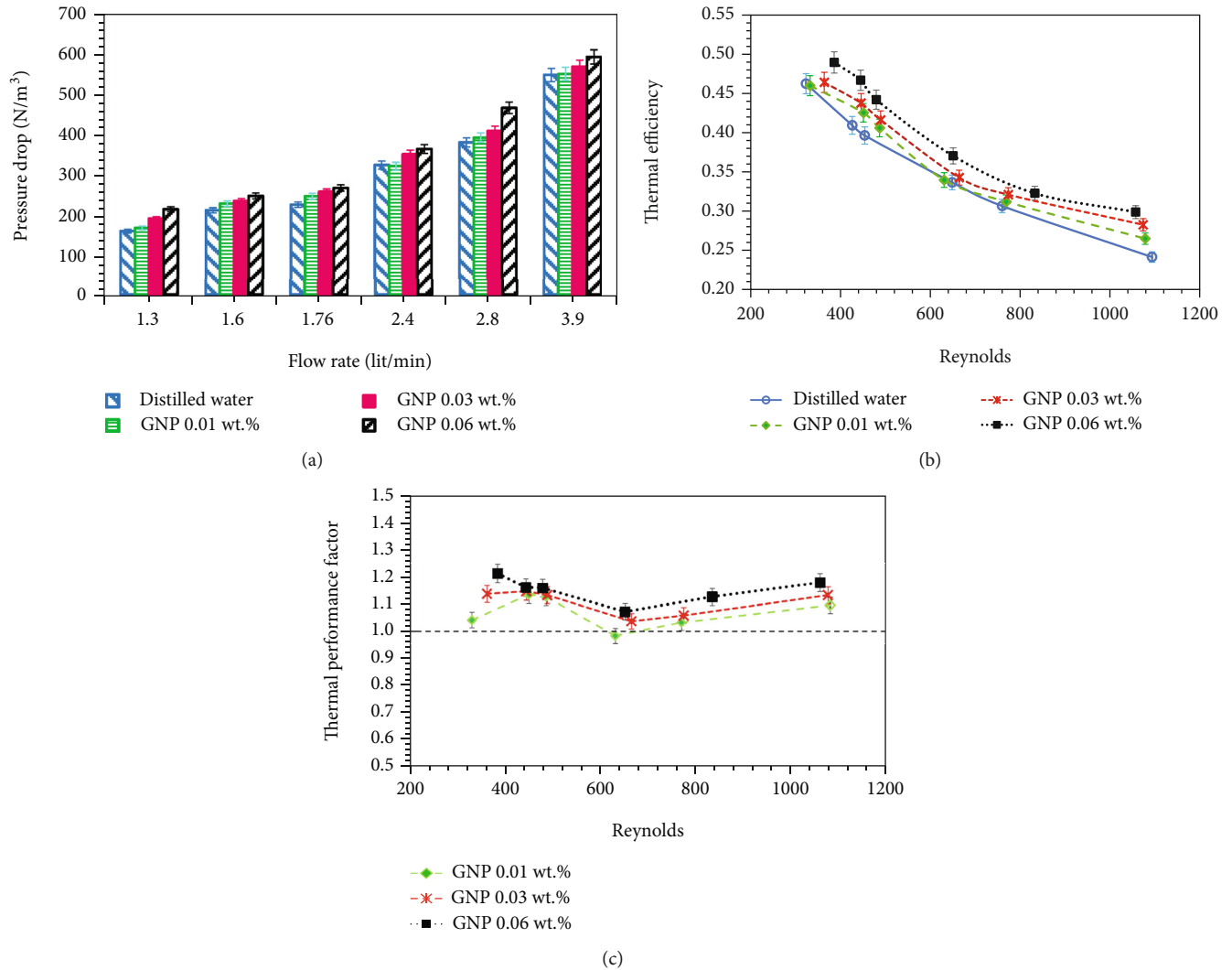


FIGURE 7: (a) Pressure drop for GNP/water nanofluid versus flow rate at different concentrations, (b) thermal efficiency versus Re at different nanofluid concentrations, and (c) thermal performance factor versus Re at different concentrations of nanofluid.

Furthermore, as Re increased from 630 to 1090 at all three concentrations, the thermal performance factor increased as turbulence, CVHTC, and heat transfer rate increased.

#### 4. Conclusion

In the first step, the characteristics of the GNP were evaluated with XRD and TEM analyses. GNP/water nanofluids were synthesized at various mass fractions (0.01 wt.%, 0.03 wt.%, and 0.06 wt.%), and the stability of the nanofluids was investigated with DLS, zeta potential, and camera pictures at different times. Secondly, the impact of GNP/water nanofluids with the various mass fractions of GNP on the thermal efficiency, thermal performance factor, pressure drop, overall heat transfer, CVHTC, and Nu was evaluated. In this research, according to findings, by adding nanoparticles, better and acceptable results were obtained in that the thermal properties were improved, which was the aim of this work to improve these properties.

- (1) The planar and layered structures of the GNP sample, along with the wrinkles on the surface layer, were clearly defined
- (2) Visual observations revealed that nanofluids with lower concentrations of 0.01 wt.% and 0.03 wt.% had good stability for up to 30 days with only minor precipitation
- (3) The zeta potential of the nanofluid was less than -27.8 mV, indicating good stability
- (4) The results illustrated that the experimental data for distilled water had a reasonably good agreement with Sieder-Tate correlation
- (5) The values of CVHTC, OHTC, and Nu at a concentration of 0.06 wt.% improved by 22.47%, 22.6%, and 12.36%, respectively
- (6) The heat transfer rate of nanofluids at a concentration of 0.06 wt.% improved by 15.66%

- (7) The thermal efficiency of the STHE was 49% at the lowest flow rate and concentration of 0.06 wt.%, which was an improvement of 8.88% over the base fluid
- (8) At low Re, the increase and decrease of the thermal performance factor were influenced by the nanofluid concentration
- (9) At high Re, the increase in thermal performance factor was affected by increased turbulence, while the decrease in thermal performance factor was affected by increased friction and the pressure drop

## Nomenclature

A:	Heat transfer rate ( $m^2$ )
Ag:	Silver
Al:	Aluminum
$C_p$ :	Specific heat (J/kg.K)
CVHTC:	Convective heat transfer coefficient
Cu:	Copper
CuO:	Copper oxide
$D$ :	Hydraulic diameter (m)
DLS:	Dynamic light scattering
EDX:	Energy dispersive X-ray
$Fe_3O_4$ :	Magnetite
GNPs:	Graphene nanoplatelets
$h$ :	Convective heat transfer coefficient (CVHTC) ( $W/m^2.K$ )
HEs:	Heat exchangers
$k$ :	Thermal conductivity ( $W/m.K$ )
$L$ :	Length of tube (m)
LMTD:	Logarithmic mean temperature difference ( $^{\circ}C$ )
$\dot{m}$ :	Mass flow rate (kg/s)
$N$ :	Number of tubes
Nu:	Nusselt number
$MoS_2$ :	Molybdenum disulphide
OHTC:	Overall heat transfer coefficient
Pe:	Peclet number
Pr:	Prandtl number
$Q$ :	Heat transfer rate (W)
$R$ :	Quantity calculated from measurable parameters
Re:	Reynolds number
STHEs:	Shell-and-tube heat exchangers
$T$ :	Temperature ( $^{\circ}C$ )
TEM:	Transmission electron microscopy
$TiO_2$ :	Titanium dioxide
$U$ :	Overall heat transfer coefficient (OHTC) ( $W/m^2.K$ )
$U_{xi}$ :	Measurement error
$U_{Ri}$ :	Maximum error
$\dot{V}$ :	Volumetric flow rate (lit/min)
XRD:	X-ray diffraction
$X_i$ :	Measurable parameter
ZnO:	Zinc oxide.

## Greek Symbols

$\varphi$ : Volume fraction (-)

$\rho$ : Density ( $kg/m^3$ )  
 $\mu$ : Viscosity ( $kg/m.s$ )  
 $\mathcal{E}$ : Thermal efficiency (-).

## Subscripts

b: Bulk  
 bf: Base fluid  
 c: Cold  
 f: Fluid  
 h: Hot  
 i: Inside  
 in: Inlet  
 nf: Nanofluid  
 np: Nanoparticle  
 o: Outside  
 out: Outlet  
 w: Wall.

## Data Availability

All data generated or analyzed during this study are included in this published article.

## Additional Points

*Highlights.* (i) The GNPs/water nanofluid was synthesised. (ii) The convective heat transfer was increased in all the concentrations of nanoparticles. (iii) The heat transfer rate of nanofluids at 0.06 wt.% improved by 15.66%. (iv) The Nu of nanofluids with 0.06 wt.% of nanoparticles improved by 12.36%

## Conflicts of Interest

The authors declare that they have no conflicts of interest.

## References

- [1] M. Heidari, S. B. Mousavi, F. Rahmani, P. T. Clough, and S. Ozmen, "The novel carbon nanotube-assisted development of highly porous CaZrO<sub>3</sub>-CaO xerogel with boosted sorption activity towards high-temperature cyclic CO<sub>2</sub> capture," *Energy Conversion and Management*, vol. 274, article 116461, 2022.
- [2] M. Iranvandi, M. Tahmasebpoor, B. Azimi, M. Heidari, and C. Pevida, "The novel SiO<sub>2</sub>-decorated highly robust waste-derived activated carbon with homogeneous fluidity for the CO<sub>2</sub> capture process," *Separation and Purification Technology*, vol. 306, article 122625, 2023.
- [3] B. Farajollahi, S. G. Etemad, and M. Hojjat, "Heat transfer of nanofluids in a shell and tube heat exchanger," *International Journal of Heat and Mass Transfer*, vol. 53, no. 1-3, pp. 12-17, 2010.
- [4] J. Yu, L. Su, K. Li, and Y. Fang, "An investigation on dehumidification and heat transfer characteristics of a minichannel heat exchanger for heat pump system of electric vehicles," *International Journal of Energy Research*, vol. 46, no. 13, pp. 18294-18311, 2022.
- [5] M. Zaboli, S. Saedodin, S. S. Mousavi Ajarostaghi, and M. Nourbakhsh, "Numerical evaluation of the heat transfer in a shell and corrugated coil tube heat exchanger with three various water-based nanofluids," *Heat Transfer*, vol. 50, no. 6, pp. 6043-6067, 2021.

- [6] Y. Wang, H. A. Al-Saaidi, M. Kong, and J. L. Alvarado, "Thermophysical performance of graphene based aqueous nanofluids," *International Journal of Heat and Mass Transfer*, vol. 119, pp. 408–417, 2018.
- [7] Y. Ma, R. Mohebbi, M. M. Rashidi, and Z. Yang, "MHD convective heat transfer of Ag-MgO/water hybrid nanofluid in a channel with active heaters and coolers," *International Journal of Heat and Mass Transfer*, vol. 137, pp. 714–726, 2019.
- [8] Z. Guo, Y. Zhang, J. Wang et al., "Interactions of Cu nanoparticles with conventional lubricant additives on tribological performance and some physicochemical properties of an ester base oil," *Tribology International*, vol. 141, article 105941, 2020.
- [9] M. Jafarian, M. Delgado, M. Omid, M. Khanali, M. Mokhtari, and A. Lázaro, "Enhancing thermophysical properties of phase change material via alumina and copper nanoparticles," *International Journal of Energy Research*, vol. 46, no. 5, pp. 6594–6612, 2022.
- [10] Z. Said, P. Sharma, L. S. Sundar, and V. D. Tran, "Using Bayesian optimization and ensemble boosted regression trees for optimizing thermal performance of solar flat plate collector under thermosyphon condition employing MWCNT-Fe<sub>3</sub>O<sub>4</sub>/water hybrid nanofluids," *Sustainable Energy Technologies and Assessments*, vol. 53, article 102708, 2022.
- [11] Z. Said, P. Sharma, L. S. Sundar et al., "Improving the thermal efficiency of a solar flat plate collector using MWCNT-Fe<sub>3</sub>O<sub>4</sub>/water hybrid nanofluids and ensemble machine learning," *Case Studies in Thermal Engineering*, vol. 40, article 102448, 2022.
- [12] S. Nejatbakhsh, H. Aghdasinia, M. Ebrahimi Farshchi, B. Azimi, and A. Karimi, "Adsorptive desulfurization of liquid hydrocarbons utilizing granular Cu/Cr-BDC@ $\gamma$ -Al<sub>2</sub>O<sub>3</sub> bimetal-organic frameworks," *Industrial & Engineering Chemistry Research*, vol. 61, no. 32, pp. 11617–11627, 2022.
- [13] A. Khataee, M. E. Farshchi, M. Fathinia, and H. Aghdasinia, "Photocatalytic ozonation process for degradation of an anthelmintic drug using ceramic coated TiO<sub>2</sub> NPs: CFD simulation coupling with kinetic mechanisms," *Process Safety and Environmental Protection*, vol. 141, pp. 37–48, 2020.
- [14] T. Huq, H. C. Ong, B. T. Chew, K. Y. Leong, and K. S. Newaz, "Review on aqueous graphene nanoplatelet nanofluids: preparation, stability, thermophysical properties, and applications in heat exchangers and solar thermal collectors," *Applied Thermal Engineering*, vol. 210, article 118342, 2022.
- [15] Z. Said, S. Rahman, P. Sharma, A. A. Hachicha, and S. Issa, "Performance characterization of a solar-powered shell and tube heat exchanger utilizing MWCNTs/water-based nanofluids: an experimental, numerical, and artificial intelligence approach," *Applied Thermal Engineering*, vol. 212, article 118633, 2022.
- [16] K. Natesan, S. V. Kodathu, and R. Verma, "Effect of graphene on the performance of heat exchangers and related simulation studies," *Materials Today: Proceedings*, vol. 46, pp. 8359–8365, 2021.
- [17] E. C. Okonkwo, I. Wole-Osho, I. W. Almanassra, Y. M. Abdulatif, and T. Al-Ansari, "An updated review of nanofluids in various heat transfer devices," *Journal of Thermal Analysis and Calorimetry*, vol. 145, no. 6, pp. 2817–2872, 2021.
- [18] G. Jiang, H. Zhu, X. Zhang et al., "Core/shell face-centered tetragonal FePd/Pd nanoparticles as an efficient non-Pt catalyst for the oxygen reduction reaction," *ACS Nano*, vol. 9, no. 11, pp. 11014–11022, 2015.
- [19] J. F. De Carvalho, S. N. De Medeiros, M. A. Morales, A. L. Dantas, and A. S. Carriço, "Synthesis of magnetite nanoparticles by high energy ball milling," *Applied Surface Science*, vol. 275, pp. 84–87, 2013.
- [20] N. G. Semaltianos, "Nanoparticles by laser ablation," *Critical reviews in solid state and materials sciences*, vol. 35, no. 2, pp. 105–124, 2010.
- [21] M. Kargaran, H. R. Goshayeshi, H. Pourpasha, I. Chaer, and S. Z. Heris, "An extensive review on the latest developments of using oscillating heat pipe on cooling of photovoltaic thermal system," *Thermal Science and Engineering Progress*, p. 101489, 2022.
- [22] B. Richard, J. L. Lemyre, and A. M. Ritcey, "Nanoparticle size control in microemulsion synthesis," *Langmuir*, vol. 33, no. 19, pp. 4748–4757, 2017.
- [23] M. Parashar, V. K. Shukla, and R. Singh, "Metal oxides nanoparticles via sol-gel method: a review on synthesis, characterization and applications," *Journal of Materials Science: Materials in Electronics*, vol. 31, no. 5, pp. 3729–3749, 2020.
- [24] J. Mayandi, R. K. Madathil, C. Abinaya et al., "Al-doped ZnO prepared by co-precipitation method and its thermoelectric characteristics," *Materials Letters*, vol. 288, article 129352, 2021.
- [25] H. Younes, M. Mao, S. S. Murshed, D. Lou, H. Hong, and G. P. Peterson, "Nanofluids: key parameters to enhance thermal conductivity and its applications," *Applied Thermal Engineering*, vol. 207, article 118202, 2022.
- [26] A. Ghozatloo, A. Rashidi, and M. Shariaty-Niassar, "Convective heat transfer enhancement of graphene nanofluids in shell and tube heat exchanger," *Experimental Thermal and Fluid Science*, vol. 53, pp. 136–141, 2014.
- [27] C. Selvam, R. S. Raja, D. M. Lal, and S. Harish, "Overall heat transfer coefficient improvement of an automobile radiator with graphene based suspensions," *International Journal of Heat and Mass Transfer*, vol. 115, pp. 580–588, 2017.
- [28] Z. Wang, Z. Wu, F. Han, L. Wadsö, and B. Sundén, "Experimental comparative evaluation of a graphene nanofluid coolant in miniature plate heat exchanger," *International Journal of Thermal Sciences*, vol. 130, pp. 148–156, 2018.
- [29] M. R. Esfahani and E. M. Languri, "Exergy analysis of a shell-and-tube heat exchanger using graphene oxide nanofluids," *Experimental Thermal and Fluid Science*, vol. 83, pp. 100–106, 2017.
- [30] N. Kumar and S. S. Sonawane, "Experimental study of Fe<sub>2</sub>O<sub>3</sub>/water and Fe<sub>2</sub>O<sub>3</sub>/ethylene glycol nanofluid heat transfer enhancement in a shell and tube heat exchanger," *International Communications in Heat and Mass Transfer*, vol. 78, pp. 277–284, 2016.
- [31] R. Barzegarian, A. Aloueyan, and T. Yousefi, "Thermal performance augmentation using water based Al<sub>2</sub>O<sub>3</sub>-gamma nanofluid in a horizontal shell and tube heat exchanger under forced circulation," *International Communications in Heat and Mass Transfer*, vol. 86, pp. 52–59, 2017.
- [32] I. M. Shahrul, I. M. Mahbulbul, R. Saidur, and M. F. Sabri, "Experimental investigation on Al<sub>2</sub>O<sub>3</sub>-W, SiO<sub>2</sub>-W and ZnO-W nanofluids and their application in a shell and tube heat exchanger," *International Journal of Heat and Mass Transfer*, vol. 97, pp. 547–558, 2016.
- [33] A. M. Hassaan, "An investigation for the performance of the using of nanofluids in shell and tube heat exchanger," *International Journal of Thermal Sciences*, vol. 177, article 107569, 2022.

- [34] Z. Taghizadeh-Tabari, S. Z. Heris, M. Moradi, and M. Kahani, "The study on application of  $\text{TiO}_2$ /water nanofluid in plate heat exchanger of milk pasteurization industries," *Renewable and Sustainable Energy Reviews*, vol. 58, pp. 1318–1326, 2016.
- [35] S. Z. Heris, M. Shokrgozar, S. Poorpharhang, M. Shanbedi, and S. H. Noie, "Experimental study of heat transfer of a car radiator with CuO/ethylene glycol-water as a coolant," *Journal of Dispersion Science and Technology*, vol. 35, no. 5, pp. 677–684, 2014.
- [36] W. Yu and S. U. Choi, "The role of interfacial layers in the enhanced thermal conductivity of nanofluids: a renovated Maxwell model," *Journal of Nanoparticle Research*, vol. 5, no. 1/2, pp. 167–171, 2003.
- [37] B. C. Pak and Y. I. Cho, "Hydrodynamic and heat transfer study of dispersed fluids with submicron metallic oxide particles," *Experimental Heat Transfer an International Journal*, vol. 11, no. 2, pp. 151–170, 1998.
- [38] H. C. Brinkman, "The viscosity of concentrated suspensions and solutions," *The Journal of Chemical Physics*, vol. 20, no. 4, p. 571, 1952.
- [39] Y. Xuan and W. Roetzel, "Conceptions for heat transfer correlation of nanofluids," *International Journal of Heat and Mass Transfer*, vol. 43, no. 19, pp. 3701–3707, 2000.
- [40] Z. Said, S. M. Rahman, M. E. Assad, and A. H. Alami, "Heat transfer enhancement and life cycle analysis of a shell-and-tube heat exchanger using stable CuO/water nanofluid," *Sustainable Energy technologies and assessments*, vol. 31, pp. 306–317, 2019.
- [41] H. Pourpasha, S. Z. Heris, and M. Mohammadpourfard, "The effect of  $\text{TiO}_2$  doped multi-walled carbon nanotubes synthesis on the thermophysical and heat transfer properties of transformer oil: a comprehensive experimental study," *Case Studies in Thermal Engineering*, vol. 41, article 102607, 2023.
- [42] H. Pourpasha, S. Z. Heris, O. Mahian, and S. Wongwises, "The effect of multi-wall carbon nanotubes/turbine meter oil nanofluid concentration on the thermophysical properties of lubricants," *Powder technology*, vol. 367, pp. 133–142, 2020.
- [43] M. Bahiraei, M. Naseri, and A. Monavari, "Thermal-hydraulic performance of a nanofluid in a shell-and-tube heat exchanger equipped with new trapezoidal inclined baffles: nanoparticle shape effect," *Powder Technology*, vol. 395, pp. 348–359, 2022.
- [44] E. Vengadesan, S. Thameenansari, E. J. Manikandan, and R. Senthil, "Experimental study on heat transfer enhancement of parabolic trough solar collector using a rectangular channel receiver," *Journal of the Taiwan Institute of Chemical Engineers*, vol. 135, article 104361, 2022.
- [45] A. V. Moghadam, H. R. Goshayeshi, I. Chaer, A. Paurine, S. Zeinali Heris, and H. Pourpasha, "Experimental investigation of multiwall carbon nanotubes/water nanofluid pool boiling on smooth and groove surfaces," *International Journal of Energy Research*, vol. 46, no. 14, pp. 19882–19893, 2022.
- [46] E. N. Sieder and G. E. Tate, "Heat transfer and pressure drop of liquids in tubes," *Industrial & Engineering Chemistry*, vol. 28, no. 12, pp. 1429–1435, 1936.
- [47] R. K. Shah, "Thermal entry length solutions for the circular tube and parallel plates," in *Proceedings of 3rd National Heat and Mass Transfer Conference*, vol. 1, pp. 11–75, Delhi, 1975 Dec.
- [48] H. Hausen, "Neue Gleichungen für die Wärmeübertragung bei freier oder erzwungener Stromung," *Allg. Waermetech*, vol. 9, pp. 75–79, 1959.
- [49] R. Siburian, H. Sihotang, S. L. Raja, M. Supeno, and C. Simanjuntak, "New route to synthesize of graphene nano sheets," *Oriental Journal of Chemistry*, vol. 34, no. 1, pp. 182–187, 2018.
- [50] R. Siburian, D. R. Sari, J. Gultom, H. Sihotang, S. L. Raja, and M. Supeno, "Performance of graphite and graphene as electrodes in primary cell battery," *Journal of Physics: Conference Series*, vol. 1116, article 042034, 2018.
- [51] M. Fares, A. M. Mohammad, and A. S. Mohammed, "Heat transfer analysis of a shell and tube heat exchanger operated with graphene nanofluids," *Case Studies in Thermal Engineering*, vol. 18, article 100584, 2020.